LETTERS
PUBLISHED ONLINE: 16 MARCH 2014 | DOI: 10.1038/NNANO.2014.29
nature nanotechnology

Engineering bright sub-10-nm upconverting nanocrystals for single-molecule imaging

Daniel J. Gargas‡, Emory M. Chan‡, Alexis D. Ostrowski†, Shaul Aloni, M. Virginia P. Altoe, Edward S. Barnard, Babak Sanii†, Jeffrey J. Urban, Delia J. Milliron, Bruce E. Cohen* and P. James Schuck*

Imaging at the single-molecule level reveals heterogeneities that are lost in ensemble imaging experiments, but an ongoing challenge is the development of luminescent probes with the photostability, brightness and continuous emission necessary for single-molecule microscopy[1–6]. Lanthanide-doped upconverting nanoparticles overcome problems of photostability and continuous emission[7–12] and their upconverted emission can be excited with near-infrared light at powers orders of magnitude lower than those required for conventional multiphoton probes[13,14]. However, the brightness of upconverting nanoparticles has been limited by open questions about energy transfer and relaxation within individual nanocrystals and unavoidable tradeoffs between brightness and size[15–18]. Here, we develop upconverting nanoparticles under 10 nm in diameter that are over an order of magnitude brighter under single-particle imaging conditions than existing compositions, allowing us to visualize single upconverting nanoparticles as small ($d = 4.8$ nm) as fluorescent proteins. We use advanced single-particle characterization and theoretical modelling to find that surface effects become critical at diameters under 20 nm and that the fluences used in single-molecule imaging change the dominant determinants of nanocrystal brightness. These results demonstrate that factors known to increase brightness in bulk experiments lose importance at higher excitation powers and that, paradoxically, the brightest probes under single-molecule excitation are barely luminescent at the ensemble level.

Lanthanide-doped upconverting nanoparticles (UCNPs) absorb multiple photons in the near infrared (NIR) and emit at higher energies in the NIR or visible (Fig. 1a). They demonstrate significant advantages over other luminescent reporters, and have therefore generated much excitement[7,8]. These include an absence of on–off blinking, single-molecule multiphoton NIR excitation at powers approaching those used for standard one-photon confocal imaging (Fig. 1b)[19], no overlap with cellular autofluorescence, and no measurable photobleaching under prolonged single-particle excitation[9–12]. Recent synthetic efforts have established control over UCNP size to produce smaller nanocrystals more compatible with many imaging applications[15,16], but this size reduction also significantly reduces brightness because surface losses increase in importance while the number of sensitizer and emitter ions per particle are reduced as d^3. UCNPs make use of energy transfer upconversion (ETU), in which sensitizer ions with relatively large absorption cross-sections sequentially transfer absorbed energy to emitter ions, which luminesce (Fig. 1a, Supplementary Fig. 1). The most common upconverting nanocrystal composition is β-phase $NaYF_4$ doped with 20% Yb^{3+} sensitizer and ~2% Er^{3+} emitter; these concentrations, in both bulk materials[20,21] and nanocrystals[3,22], have been suggested to optimize brightness by increasing photon absorption and minimizing luminescence quenching.

Recent work on larger nanocrystals ($d \approx 40$ nm) has shown improvements in brightness with higher emitter concentrations at high excitation irradiance[18]. The photophysical processes leading to luminescence quenching in larger nanocrystals and in bulk are related primarily to cross-relaxation between dopants and energy migration to defects, but it is less clear how these kinetics are modified as nanocrystal sizes drop to single-digit diameters. To understand the efficiency of the ETU process in these UCNPs and the

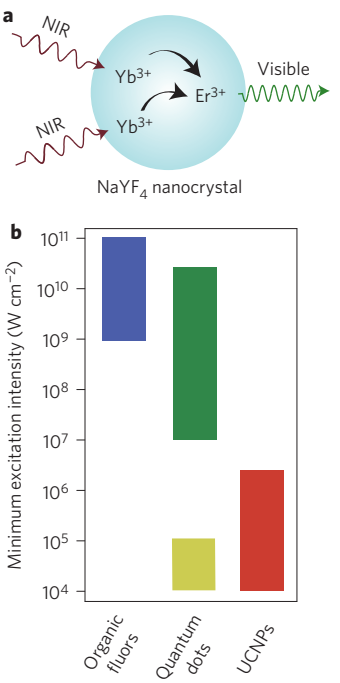

Figure 1 | Luminescence of UCNPs. a, Schematic of energy transfer upconversion with Yb^{3+} as sensitizer and Er^{3+} as emitter. **b**, Minimum peak excitation intensities of NIR light needed for multiphoton single-molecule imaging of various classes of luminescent probes. The peak excitation intensity ranges shown are required to detect signals of ~100 c.p.s. for core–shell quantum dots (green, ref. 13), 40 nm colloidal double dot-rods (yellow, ref. 34), organic fluorophores[14] and UCNPs (this study and refs 8,16).

Molecular Foundry, Lawrence Berkeley National Laboratory, Berkeley, California 94720, USA, †Present address: Department of Chemistry, Bowling Green State University, Bowling Green, Ohio 43403, USA (A.D.O.), W.M. Keck Science Department, Claremont-McKenna College, Claremont, California 91711, USA (B.S.). ‡These authors contributed equally to this work. *e-mail: becohen@lbl.gov; pjschuck@lbl.gov

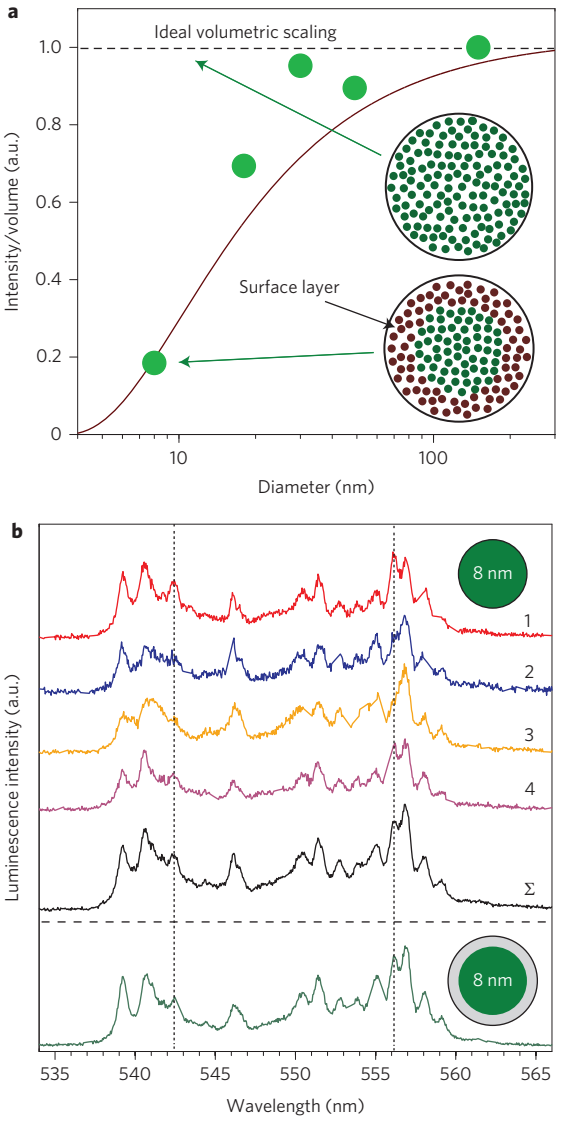

Figure 2 | UCNP size-dependent luminescence intensity and heterogeneity. **a**, Deviation of single UCNP luminescence intensity normalized to particle volume from ideal volumetric scaling ($n = 300$ total). The curve represents calculated intensity normalized to volume for UCNPs with a non-luminescent surface layer of 1.7 nm. Only intensities from single, unaggregated nanocrystals, as determined by Supplementary Fig. 5, are used. The top inset shows a diagram representing an ideal nanocrystal in which with all included emitters are luminescent (green circles). The bottom inset is a diagram representing a nanocrystal with emitters that are non-luminescent (maroon circles) in an outer surface layer. **b**, Fine spectra of the green emission bands collected from four single 8 nm UCNPs (curves 1–4) and their averaged spectra (curve Σ). Vertical dotted lines highlight peaks exhibiting heterogeneity between individual UCNPs. The green emission spectrum of an 8 nm UCNP with epitaxial 1.8 nm undoped shell is shown below the horizontal dashed line.

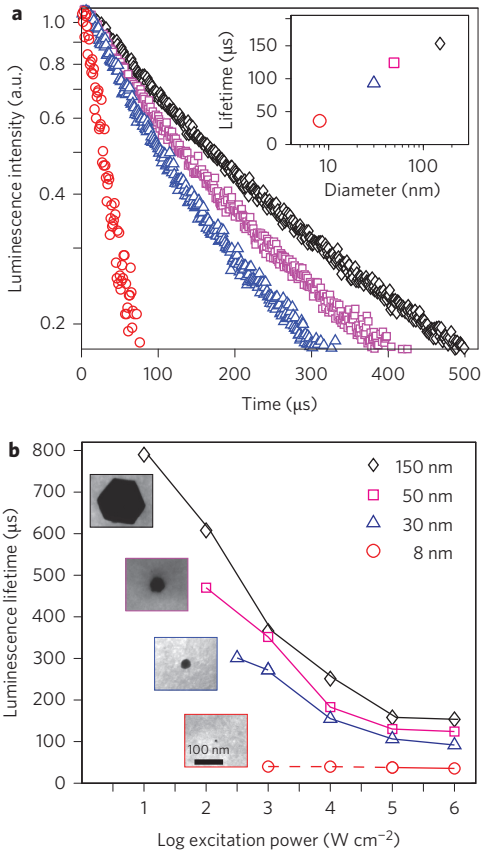

Figure 3 | Single UCNP luminescence lifetime as a function of particle size and excitation power. **a**, Luminescence decay (normalized) plotted for various UCNP diameters. See Supplementary Fig. 10 for full lifetime curves. Inset: Lifetime values plotted as a function of UCNP diameter. They were determined by fitting luminescence decay curves to a double exponential and plotting only the dominant decay value. **b**, Single UCNP lifetime values for various diameters plotted as a function of excitation power. In these plots, emission from all wavelengths between 532 nm and 700 nm was used for the fit because the trends were the same for all emission bands in this range. Separate fits for just green and red emission were also collected and are discussed in Supplementary Figs 7 and 8 and Supplementary Table 1. For simplicity, only dominant lifetime decay values are plotted. Dashed line represents data collected from 8 nm UCNP clusters. Insets are scanning transmission electron microscopy (STEM) images of single UCNPs with 8 nm, 30 nm, 50 nm and 150 nm diameters.

potential sources of energy loss associated with the nanocrystal surface, we investigated the size-dependent luminescence intensity distributions of single UCNPs (Fig. 2 and Supplementary Figs 2–5). Even under the dilute conditions used to prepare samples for single nanocrystal measurements, we note the presence, in scanning electron microscopy (SEM) images, of a small fraction of dimers and other aggregates (Supplementary Fig. 5). In Fig. 2 and throughout this study, we use emission only from single, non-aggregated nanocrystals, which is critical to understanding the size- and surface-dependent UCNP photophysics, and which may be compromised in ensemble measurements. For larger UCNPs ($d > 20$ nm), emission intensity scales linearly with particle volume, but at smaller sizes, surface-related losses become significant, reducing brightness below that predicted for ideal volumetric scaling (Fig. 2a). This trend is consistent with recent ensemble measurements on sub-10-nm UCNPs[23,24], and these data can be analysed using a simple calculation in which the UCNP is divided into two regions: a dark surface region and a luminescent core region. In the context of this calculation, our data indicate the dark surface radius is ~1.7 nm (ref. 25), because the observed intensity of the 8 nm particles is equivalent to the extrapolated intensity of an ~4.6-nm-diameter particle assuming ideal volumetric scaling.

To understand the origins of these surface-related losses, we collected visible emission spectra from approximately 40 individual 8 nm UCNPs. Unlike homogeneous room-temperature spectra of larger UCNPs[3], these high-resolution spectra are heterogeneous, with particle-to-particle variations in peak intensities at 541 and

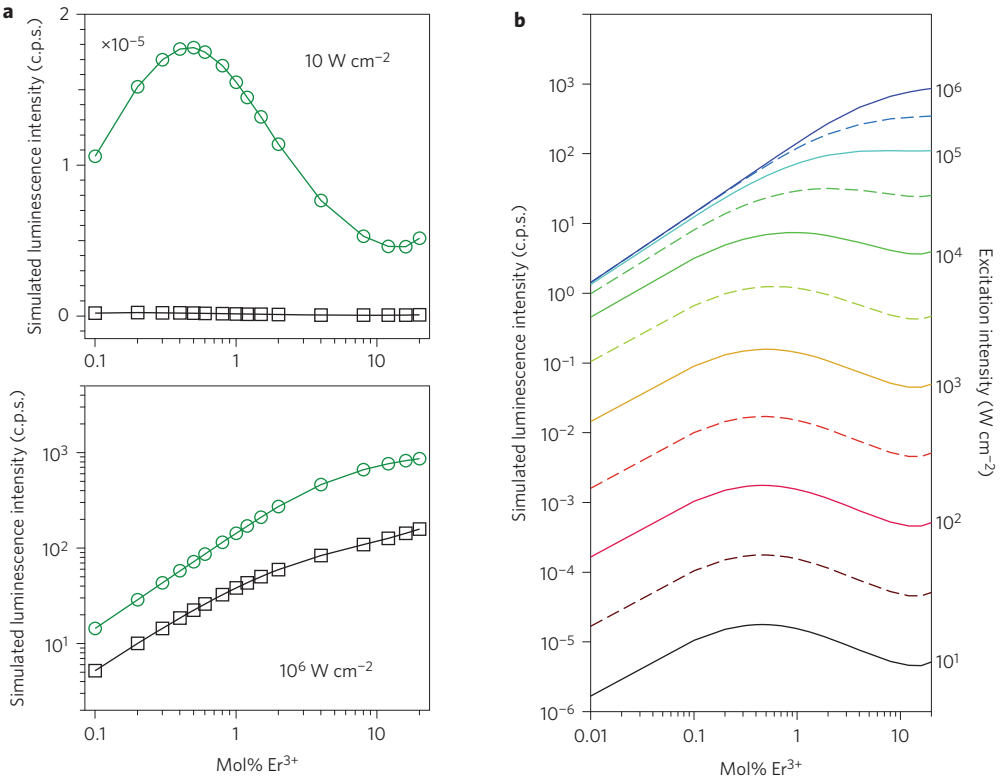

Figure 4 | Simulated UCNP emission intensity. a, Theoretical models of integrated 8 nm UCNP emission (500–700 nm) as a function of Er^{3+} mol% for 20% Yb^{3+} (green circles) and 2% Yb^{3+} (black squares) for low (10 W cm^{-2}, upper panel) and high (10^6 W cm^{-2}, lower panel) intensity excitation. **b**, Simulated luminescence intensity of UCNPs with 20% Yb^{3+} as a function of Er^{3+} doping and excitation intensity. Solid lines are calculated UCNP emission following excitation at intensities on the right axis. Dashed lines are half logarithmic spacings.

557 nm (Fig. 2b; compare curves 1 and 4 with curves 2 and 3). One explanation for such heterogeneity would be that emission from these UCNPs is dominated by only a few of the approximately 70 Er^{3+} emitters present in each UCNP, but this is not supported by photon antibunching studies of single UCNPs (Supplementary Fig. 6). The addition of undoped $NaYF_4$ shells to these nanocrystals eliminates this heterogeneity (Fig. 2b, bottom trace) suggesting a region within the nanocrystal in which the lanthanides may be emissive but are energetically coupled to the surface. The observed spectral differences may arise from either variations in lanthanide distributions between nanocrystals, or from subtle variations in surface defects, surface reconstruction, or faceting. This identification of losses from energy transfer to the surface suggests one means for improving emission from small UCNPs.

We next measured the luminescence lifetimes of individual UCNPs of various sizes to probe the balance between the energy transfer pathways that lead to radiative and non-radiative relaxation. As UCNP size decreases, fast and presumably non-radiative recombination dominates (Fig. 3a). To determine whether surfaces are a primary source of the non-radiative relaxation, we measured the lifetimes of 8 nm UCNP cores with added undoped $NaYF_4$ shells. Emission intensities and lifetimes both increase as shell thickness increases, up to a shell thickness of ~1.8 nm (Supplementary Fig. 11), suggesting that the increased luminescence is due to improved quantum yields for core–shell nanocrystals[16,26]. This saturation of lifetime and brightness at a shell thickness of ~1.8 nm is consistent with a model (Fig. 2a) in which the emitters within this surface radius are quenched by energy transfer to vibrational modes at the nanocrystal surface or in organic capping ligands. Because dopant excited states can be coupled to surface vibrations directly or via resonant, donor-to-donor energy migration to directly coupled states, this ~1.8 nm distance can be interpreted physically as a convolution of the critical distance for direct coupling and the average energy migration length (Supplementary Discussion 1). Critically, for UCNPs with $d < 8$ nm, this dark surface layer occupies a large majority (>80%) of the total nanocrystal volume.

Previous work has shown that UCNP lifetimes are roughly independent of excitation power for powers <100 W cm^{-2} (ref. 25), but the low power densities used in those experiments are not useful for imaging small, single UCNPs. At higher single-nanocrystal powers, we observe a pronounced lifetime dependence on excitation power density for all UCNPs with $d > 30$ nm (Fig. 3b). We considered the possibility that these higher powers may generate enough heat to significantly affect lifetimes, although we observed no change in lifetime for any UCNPs as pump pulse widths were increased from 250 μs to 2.5 ms, indicating that the particles reach a steady-state temperature in less than 250 μs. Rather, the lifetime dependence on excitation power suggests that the higher fluences increase the spatial density of populated Er^{3+} excited states with longer lifetimes (such as $^4S_{3/2}$), increasing rates of ETU and cross-relaxation out of these states. This leads to shorter lifetimes for states that emit visible photons and increases the population of higher-energy excited states (such as $^4G_{11/2}$)[27]. However, for the sub-10-nm UCNPs, the luminescence lifetime is short and remains constant for all excitation powers studied here (Fig. 3b), due to the dominance of surface-related non-radiative recombination in UCNPs of this size. This suggests that the entire 8 nm particle is energetically coupled to the surface—although the nanocrystal radius is larger than the dark radius of 1.7 nm—and is consistent with the presence of the sub-surface region containing emissive lanthanides that are nonetheless influenced by the surface.

Surface-related non-radiative recombination greatly shortens the lifetime of excited emitters, which suggests an opportunity in that emitter concentrations could be increased substantially beyond 2%

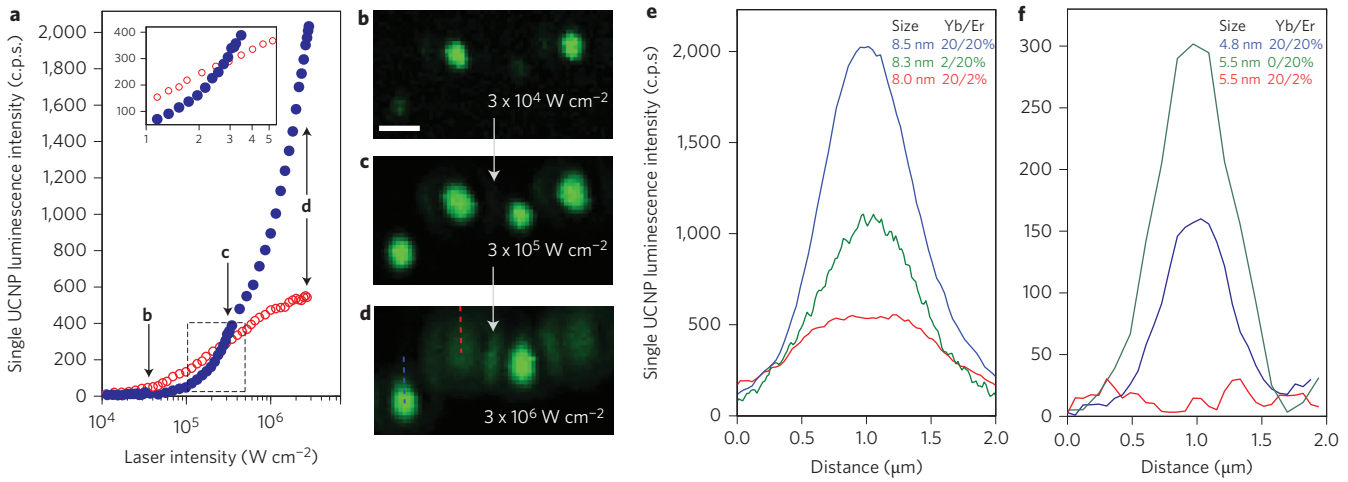

Figure 5 | Luminescence intensity of single UCNPs as a function of Er^{3+} and Yb^{3+} doping. a, Luminescence intensity of single 8 nm UCNPs with 20% (blue circles) and 2% (red circles) Er^{3+}, each with 20%Yb^{3+}, plotted as a function of excitation intensity. Inset: zoom-in of the luminescence intensity cross-over region for UCNPs with the two different emitter concentrations. **b**–**d**, Confocal luminescence images taken at points shown in **a** of single UCNPs containing a mixture of 2% and 20% Er^{3+}. The images were collected at increasing excitation intensities. Dashed lines indicate regions from which luminescence intensity was collected for data in **a**. Scale bar, 1 μm. **e**,**f**, Linecuts of single-particle luminescence scans of ~8 nm UCNPs and ~5 nm UCNPs with varying Er^{3+} and Yb^{3+} doping levels. Yb and Er levels are given in atomic %. Emission from 5.5 nm UCNPs with 20% Yb^{3+} and 2% Er^{3+} are indistinguishable from our sensitivity limit determined by instrument noise. These data were collected using 3×10^6 W cm^{-2} excitation intensity and a ×100, 1.4 numerical aperture oil-immersion lens (see Methods and Supplementary Fig. 2 for details).

before self-quenching becomes a major factor. In this case, the surface energy losses change the relative balance between energy transfer pathways in smaller UCNPs. In addition, the higher fluences of single-molecule imaging push the nanocrystals into the excitation saturation regime and further modify the balance of energy transfer between states[18]. These findings suggest that the optimal design has not yet been achieved for sub-10-nm UCNPs intended for single-molecule applications, where the goal is to maximize emission over background and noise levels.

We used these observations to refine computational models of UCNP energy transfer to design UCNPs that are brighter under single-molecule imaging conditions. Emission intensity was calculated as a function of Er^{3+} and Yb^{3+} dopant concentrations using a population balance model that has successfully predicted the steady-state luminescence spectra of various lanthanide-doped UCNPs[28]. Based on the single-nanocrystal intensity and lifetime data, we modified this model to include a third, non-emissive surface species that can accept energy from excited lanthanide states (Supplementary Methods 1). At the low excitation powers typical of ensemble measurements (10 W cm^{-2}), the simulated emission intensity is maximized at ~0.5% Er^{3+} (Fig. 4a, top)—close to the 1–2% Er^{3+} maximum typically observed for Er^{3+}-containing nanocrystals[29]. On the other hand, increasing the Yb^{3+} concentration from 2 to 20% increases the luminescence by two orders of magnitude at all Er^{3+} concentrations. However, when we apply the refined model to the higher powers (10^5–10^7 W cm^{-2}) needed to observe single small nanocrystals, we find that the sensitizer Yb^{3+} $^2F_{5/2}$ excited manifold has its population approach 70% of the overall Yb^{3+} ion concentration, well into the saturation regime (Supplementary Fig. 14). At these higher fluences, the incremental Yb^{3+} absorption cross-section decreases significantly[19], thereby resulting in a reduced dependence of emission on Yb^{3+} sensitizer concentration (Fig. 4a, bottom). The number of Er^{3+} emitters becomes the fundamental bottleneck for visible emission (Fig. 4b and Supplementary Discussion 2) because radiative relaxation rates for parity-forbidden 4*f*-to-4*f* transitions are significantly slower than photon absorption rates in this regime. Luminescence increases linearly as a function of Er^{3+} doping percentage (Fig. 4b), because the emission intensity is proportional to the number of Er^{3+} states that can emit visible photons (for example, $^4S_{3/2}$, $^4F_{9/2}$)[28], as well as the number of Er^{3+} ions that can absorb incident photons. This model predicts that a UCNP with 20% Er^{3+} will be three to five times brighter at higher excitation fluences than a conventional 2% Er^{3+} UCNP of the same size and that Yb^{3+} doping levels are of less importance than at lower fluences.

This points to a radically different design strategy for nanocrystals to be used for ensemble measurements versus those to be used for single-molecule studies: for single-molecule studies, emitter concentrations should be as high as possible without compromising the structure of the nanocrystal, while sensitizer content becomes less significant at higher powers and can potentially be eliminated for single-molecule imaging applications. Based on these calculations, we synthesized a series of 8 nm and 5 nm nanocrystals with higher emitter or lower activator content, and imaged them at single-particle powers (Fig. 5). At lower powers (~100 W cm^{-2}), these new compositions have vanishingly low quantum yields (Supplementary Table 4), indicating that they would behave poorly in ensemble imaging experiments. However, comparing β-$NaYF_4$ nanocrystals doped with 20% Yb^{3+} and 20% Er^{3+} (as well as 25% Gd^{3+} added to maintain β-phase morphology at high lanthanide doping levels[7]) to conventional 8 nm UCNPs (β-$NaYF_4$ with 20% Yb^{3+} and 2% Er^{3+}) dispersed on the same glass substrate, we observe that the conventional UCNPs are visible at lower powers, but the high-Er^{3+} UCNPs are not (Fig. 5a–d). As excitation powers are raised, the conventional UCNPs saturate in brightness while the high-Er^{3+} UCNPs become visible and continue to increase in brightness, surpassing the conventional UCNPs. The excitation intensity at which the 20% Er^{3+} UCNPs become brighter than their 2% Er^{3+} counterparts is $\sim 3 \times 10^5$ W cm^{-2} (Fig. 5a). The diverging brightness trends of these UCNPs, which agree well with simulated data (Supplementary Fig. 14), indicate one advantage of tailoring dopant compositions specifically for higher-flux imaging. This advantage is explicitly illustrated by simultaneously imaging the two classes of UCNPs at increasing excitation intensities and also may be potentially useful in optical

encoding applications[18,30] or in conjunction with surface modifications that shift UCNP absorption or emission[31].

This strategy for increasing single-nanocrystal brightness suggests that even smaller UCNPs may be viable as single-molecule probes. We tested this idea by synthesizing 5.5-nm-diameter β-$NaYF_4$ UCNPs with 20% Er^{3+} and no Yb^{3+} sensitizer, as well as 4.8 nm UCNPs with ~20% each of Er^{3+}, Yb^{3+} and 25% Gd^{3+} (Fig. 5e,f and Supplementary Discussion 3). These nanocrystals are significantly smaller than other UCNPs imaged at the single-particle level[16,18] and are the approximate size of monomeric genetically encoded fluorescent proteins. We find that each of these compositions is significantly brighter than the canonical β-$NaYF_4$:20% Yb^{3+} 2% Er^{3+} nanocrystals. We measured signals of ~150 c.p.s. for single 4.8 nm UCNPs doped with 20% Yb^{3+} 20% Er^{3+} and note that these nanocrystals have quantum yields of <0.001% at lower excitation powers (Supplementary Table 4). In comparison, we were unable to image single 5.5 nm β-$NaYF_4$:20% Yb^{3+} 2% Er^{3+} nanocrystals because their signal falls below our sensitivity limit of ~25 c.p.s. (Fig. 5f, Supplementary Fig. 12). The 4.8 nm UCNPs with 20% Yb^{3+} and 20% Er^{3+} are over 500-fold smaller in volume than nanocrystals optimized with higher emitter concentrations for single-particle excitation irradiance and imaged as single nanocrystals in suspension[18]. These protein-sized nanocrystals have significant advantages over the larger UCNPs previously used in cellular imaging applications, including increased accessibility to small subcellular structures, greater tissue penetration and reduced interference with biomolecule function, trafficking and binding events[16].

These new rules for designing small, bright UCNPs address key obstacles for optimizing nanocrystals as single-molecule probes and suggest a single-molecule probe development strategy involving iterative rounds of kinetic modelling and detailed nanocrystal characterization. We find that factors known to increase brightness at low powers are unimportant at single-molecule powers and that the brightest single-molecule probes may be non-luminescent at the ensemble level. For the most efficient nanocrystals, we find that 5 nm UCNPs are bright enough to be used in single-molecule detection. We anticipate further gains in brightness through iterative rounds of modelling and nanocrystal characterization, as well as surface modifications that alter the balance between various energy transfer pathways[31,32]. Together, these advances open the door to a range of applications, including cellular and *in vivo* imaging[12,33], as well as reporting on local electromagnetic near-field properties of complex nanostructures.

Methods

β-$NaYF_4$:Yb^{3+}, Er^{3+} nanocrystals were synthesized as reported previously[16] and characterized by analytical transmission electron microscopy (TEM), dynamic light scattering and X-ray diffraction. UCNPs were dispersed in hexane to ~0.1 nM before dropcasting onto silicon nitride TEM grids (Ted Pella, #21569-10). Laser scanning confocal imaging was performed under ambient conditions using a 980 nm continuous-wave laser (Thorlabs TCLDM9, 300 mW diode) (see Supplementary Fig. 2 for instrument details). Because the diffraction-limited beam spot was larger than individual nanoparticle size, single particles were confirmed on SiN TEM-grid samples by subsequent SEM imaging (Zeiss Ultra-55, operating in transmission mode).

Single-particle luminescence intensity histograms were compiled from ~50–300 individual particles for each size (Supplementary Fig. 5), and single-particle spectra were obtained using the same confocal imaging system. To obtain lifetime data, a time-correlated single-photon counter (TCSPC, Picoquant) was used to tag the photon arrival times of the collected luminescence with respect to the laser operating in pulsed mode. The resulting time-resolved luminescence plots were fitted to a double exponential, because the non-radiative recombination rates from the surface and core regions of a UCNP are generally different[25]. For clarity, only the dominant decay value was plotted in Fig. 3 (Supplementary Figs 7 and 8 show more complete information).

In our optical set-up, the excitation laser was pre-focused with a 500 mm lens before entering the back-aperture of either a 0.95 NA, ×100 air objective (used for the data in Figs 2 and 3) or a 1.4 NA, ×100 oil objective (Fig. 5). Emitted light was collected with the same objective and filtered by two 700 nm short-pass filters (Chroma) to remove residual laser light. Emission was then routed either through a spectrometer, or through additional 532 nm long-pass filters, and onto a single photon-counting avalanche photodiode. To collect data from just the green or red spectral band, a 540±20 nm (green) or 650±20 nm (red) bandpass filter was used in place of the 532 nm long-pass filters. A TCSPC (Picoquant) was used for luminescence lifetime measurements.

The single-particle imaging shown in Fig. 5 was performed using a 1.4 NA, ×100 oil-immersion objective. Equal dilutions of 20/2% (Yb/Er) and 25/20/20% (Gd/Yb/Er) UCNPs were dropcast onto a glass coverslip and imaged at various powers. For mixtures of nanocrystals with different dopant compositions, the compositions were identified by comparison with the optical behaviour of each composition imaged individually (Fig. 5d). Single-particle power-dependent plots were constructed by scanning the laser beam over an isolated particle and dividing the collected luminescence curve by the laser beamspot profile, assuming Gaussian shapes. Consecutive linecut scans at increasing excitation powers were compiled to produce the plots shown in Fig. 5a. The linecuts shown in Fig. 5e,f were collected from single particles at a fixed excitation intensity of 3×10^6 W cm^{-2}.[34]

Received 30 August 2013; accepted 24 January 2014; published online 16 March 2014; corrected online 24 March 2014

References

1. Thompson, M. A., Lew, M. D. & Moerner, W. E. Extending microscopic resolution with single-molecule imaging and active control. *Annu. Rev. Biophys.* **41,** 321–342 (2012).
2. Auzel, F. Upconversion and anti-Stokes processes with *f* and *d* ions in solids. *Chem. Rev.* **104,** 139–173 (2004).
3. Haase, M. & Schafer, H. Upconverting nanoparticles. *Angew. Chem. Int. Ed.* **50,** 5808–5829 (2011).
4. Buenzli, J-C. G. Lanthanide luminescence for biomedical analyses and imaging. *Chem. Rev.* **110,** 2729–2755 (2010).
5. Park, Y. I. *et al.* Nonblinking and nonbleaching upconverting nanoparticles as an optical imaging nanoprobe and T1 magnetic resonance imaging contrast agent. *Adv. Mater.* **21,** 4467–4471 (2009).
6. Cohen, B. E. Biological imaging: beyond fluorescence. *Nature* **467,** 407–408 (2010).
7. Wang, F. *et al.* Simultaneous phase and size control of upconversion nanocrystals through lanthanide doping. *Nature* **463,** 1061–1065 (2010).
8. Wu, S. *et al.* Non-blinking and photostable upconverted luminescence from single lanthanide-doped nanocrystals. *Proc. Natl Acad. Sci. USA* **106,** 10917–10921 (2009).
9. Ryu, J. *et al.* Facile synthesis of ultrasmall and hexagonal $NaGdF_4$: Yb^{3+}, Er^{3+} nanoparticles with magnetic and upconversion imaging properties. *J. Phys. Chem. C* **114,** 21077–21082 (2010).
10. Gnach, A. & Bednarkiewicz, A. Lanthanide-doped up-converting nanoparticles: merits and challenges. *Nano Today* **7,** 532–563 (2012).
11. Van der Ende, B. M., Aarts, L. & Meijerink, A. Lanthanide ions as spectral converters for solar cells. *Phys. Chem. Chem. Phys.* **11,** 11081–11095 (2009).
12. Nam, S. H. *et al.* Long-term real-time tracking of lanthanide ion doped upconverting nanoparticles in living cells. *Angew. Chem. Int. Ed.* **50,** 6093–6097 (2011).
13. Jauffred, L. & Oddershede, L. B. Two-photon quantum dot excitation during optical trapping. *Nano Lett.* **10,** 1927–1930 (2010).
14. Schuck, P. J., Willets, K. A., Fromm, D. P., Twieg, R. J. & Moerner, W. E. A novel fluorophore for two-photon-excited single-molecule fluorescence. *Chem. Phys.* **318,** 7–11 (2005).
15. Wang, F. *et al.* Tuning upconversion through energy migration in core–shell nanoparticles. *Nature Mater.* **10,** 968–973 (2011).
16. Ostrowski, A. D. *et al.* Controlled synthesis and single-particle imaging of bright, sub-10 nm lanthanide-doped upconverting nanocrystals. *ACS Nano* **6,** 2686–2692 (2012).
17. Schietinger, S., Menezes, L. D., Lauritzen, B. & Benson, O. Observation of size dependence in multicolor upconversion in single Yb^{3+}, Er^{3+} codoped $NaYF_4$ nanocrystals. *Nano Lett.* **9,** 2477–2481 (2009).
18. Zhao, J. *et al.* Single-nanocrystal sensitivity achieved by enhanced upconversion luminescence. *Nature Nanotech.* **8,** 729–734 (2013).
19. Moerner, W. E. & Fromm, D. P. Methods of single-molecule fluorescence spectroscopy and microscopy. *Rev. Sci. Instrum.* **74,** 3597–3619 (2003).
20. Kramer, K. W. *et al.* Hexagonal sodium yttrium fluoride based green and blue emitting upconversion phosphors. *Chem. Mater.* **16,** 1244–1251 (2004).
21. Suyver, J. F. *et al.* Upconversion spectroscopy and properties of $NaYF_4$ doped with Er^{3+}, Tm^{3+} and/or Yb^{3+}. *J. Lumin.* **117,** 1–12 (2006).
22. Yi, G. S. & Chow, G. M. Synthesis of hexagonal-phase $NaYF_4$:Yb,Er and $NaYF_4$:Yb,Tm nanocrystals with efficient up-conversion fluorescence. *Adv. Funct. Mater.* **16,** 2324–2329 (2006).
23. Chen, G. Y., Ohulchanskyy, T. Y., Kumar, R., Agren, H. & Prasad, P. N. Ultrasmall monodisperse $NaYF_4$:Yb^{3+}/Tm^{3+} nanocrystals with enhanced near-infrared to near-infrared upconversion photoluminescence. *ACS Nano* **4,** 3163–3168 (2010).

24. Lim, S. F., Ryu, W. S. & Austin, R. H. Particle size dependence of the dynamic photophysical properties of $NaYF_4$:Yb, Er nanocrystals. *Opt. Express* **18,** 2309–2316 (2010).
25. Zhao, J. *et al.* Upconversion luminescence with tunable lifetime in $NaYF_4$:Yb,Er nanocrystals: role of nanocrystal size. *Nanoscale* **5,** 944–952 (2013).
26. Wang, F., Wang, J. A. & Liu, X. G. Direct evidence of a surface quenching effect on size-dependent luminescence of upconversion nanoparticles. *Angew. Chem. Int. Ed.* **49,** 7456–7460 (2010).
27. Pollnau, M., Gamelin, D. R., Luthi, S. R., Gudel, H. U. & Hehlen, M. P. Power dependence of upconversion luminescence in lanthanide and transition-metal-ion systems. *Phys. Rev. B* **61,** 3337–3346 (2000).
28. Chan, E. M., Gargas, D. J., Schuck, P. J. & Milliron, D. J. Concentrating and recycling energy in lanthanide codopants for efficient and spectrally pure emission: the case of $NaYF_4$:Er^{3+}/Tm^{3+} upconverting nanocrystals. *J. Phys. Chem. B* **116,** 10561–10570 (2012).
29. Zeng, J. H., Su, J., Li, Z. H., Yan, R. X. & Li, Y. D. Synthesis and upconverstion luminescence of hexagonal-phase $NaYF_4$:Yb, Er^{3+} phosphors of controlled size and morphology. *Adv. Mater.* **17,** 2119–2123 (2005).
30. Downing, E., Hesselink, L., Ralston, J. & Macfarlane, R. A three-color, solid-state, three-dimensional display. *Science* **273,** 1185–1189 (1996).
31. Zou, W., Vissser, C., Maduro, J. A., Pshenichnikov, M. S. & Hummelen, J. C. Broadband dye-sensitized upconversion of near-infrared light. *Nature Photon.* **6,** 560–564 (2012).
32. Kannan, P. *et al.* Enhanced emission of $NaYF_4$:Yb,Er/Tm nanoparticles by selective growth of Au and Ag nanoshells. *RSC Adv.* **3,** 7718–7721 (2013).
33. Liu, Q. *et al.* Sub-10 nm hexagonal lanthanide-doped $NaLuF_4$ upconversion nanocrystals for sensitive bioimaging *in vivo*. *J. Am. Chem. Soc.* **133,** 17122–17125 (2011).
34. Deutsch, Z., Neeman, L. & Oron, D. Luminescence upconversion in colloidal double quantum dots. *Nature Nanotech.* **8,** 649–653 (2013).

Acknowledgements

The authors thank M. Salmeron and R. Johns for discussions and comments on the manuscript, as well as A. Nievergelt and A. Mueller for assistance with data processing and visualization. P.J.S. acknowledges Bica for support. A.D.O. was supported by a fellowship from the National Institute of Biomedical Imaging and Bioengineering, under NIH Award F32EB014680. Work at the Molecular Foundry was supported by the Director, Office of Science, Office of Basic Energy Sciences, Division of Materials Sciences and Engineering, of the US Department of Energy (contract no. DE-AC02-05CH11231).

Author contributions

P.J.S., B.E.C., D.J.M., D.J.G., E.M.C. and A.D.O. developed the idea for the project. A.D.O., E.M.C. and B.E.C. synthesized the nanocrystals. E.M.C. performed the kinetic modelling and simulations. D.J.G. performed the single-UCNP optical imaging, lifetime and spectroscopy measurements, as well as single-UCNP scanning TEM imaging. S.A. and M.V.P.A. provided TEM and analysis. J.J.U. provided in-depth discussions. E.S.B. and B.S. provided in-depth discussions and performed data analysis. D.J.G., E.M.C., B.E.C. and P.J.S. wrote the paper. All authors reviewed the paper.

Additional information

Supplementary information is available in the online version of the paper. Reprints and permissions information is available online at www.nature.com/reprints. Correspondence and requests for materials should be addressed to B.E.C. and P.J.S.

Competing financial interests

The authors declare no competing financial interests.

ERRATUM

Engineering bright sub-10-nm upconverting nanocrystals for single-molecule imaging

Daniel J. Gargas, Emory M. Chan, Alexis D. Ostrowski, Shaul Aloni, M. Virginia P. Altoe, Edward S. Barnard, Babak Sanii, Jeffrey J. Urban, Delia J. Milliron, Bruce E. Cohen and P. James Schuck

Nature Nanotechnology http://dx.doi.org/10.1038/nnano.2014.29 (2014); published online 16 March 2014;
corrected online 24 March 2014.

In the version of this Letter originally published online, in Fig. 2b caption, the last two sentences were missing. This error has now been corrected in all versions of the Letter.